Thermomechanical Enhancement of DPP-4T through Purposeful π-Conjugation Disruption

*Connor P. Callaway, Joel H. Bombile, Walker Mask, Sean M. Ryno, Chad Risko**

Department of Chemistry
and Center for Applied Energy Research
University of Kentucky
Lexington, Kentucky 40506, USA

Corresponding Author: Chad Risko, chad.risko@uky.edu

Keywords: conjugated polymers, alkyl spacers, thermomechanical properties

ORCID

Connor P. Callaway – 0000-0002-0848-1000
Joel H. Bombile – 0000-0001-9160-1343
Walker Mask – 0000-0002-0911-857X
Sean M. Ryno – 0000-0002-8359-2659
Chad Risko – 0000-0001-9838-5233

Abstract

The design of polymer-based organic semiconductors that offer mechanical deformability while maintaining efficient semiconducting characteristics remains a significant challenge. Recent synthetic efforts have incorporated small alkyl segments directly into otherwise π-conjugated polymer backbones to enhance processability, mechanical deformability, and other properties. The resulting polymers can be used as stand-alone materials or as matrix polymers in complementary semiconducting polymer blends offering reasonable charge-carrier transport properties, thermal healing, and deformability. Here, a family of diketopyrrolopyrrole-tetrathiophene (DPP-4T) variants is explored via large-scale atomistic molecular dynamics simulations to examine the effect of alkyl segments incorporated into the polymer backbone on the polymer structure, dynamics, and thermal properties. Longer alkyl segments lead to polymer chains that are more flexible, compact, and mobile, with lower glass transition temperatures for the condensed phase.

Introduction

Organic semiconductors (OSC) derived from π-conjugated polymers have attracted considerable interest for their combination of excellent optoelectronic properties with the inherent mechanical properties of plastics.[1-5] Polymers for OSC generally feature a rigid π-conjugated backbone, responsible for the electronic character of the chains with nonconjugated (often alkyl) side chains, added to enhance solubility. Chemical tuning of the backbone has historically been the primary means of controlling the electronic, redox, and optical properties of π-conjugated polymers and polymer-based semiconductors.[6-10] Within the last two decades, there has been active emphasis on using the (generally electronically insulating) side groups to regulate the solid-state polymer packing and modify the charge-carrier transport behavior.[11-13] Ultimately, however, the rational design of polymer-based OSC with pre-defined optoelectronic and mechanical properties requires refining our understanding of the relationship between the backbone and side chain chemistries of π-conjugated polymers, the intra- and inter-chain interactions of the polymers in the condensed phase, and the subsequent charge-carrier transport mechanisms.[14-32]

Efficient charge-carrier transport in polymer-based OSC is typically associated with rigid, torsionally robust π-conjugated backbones.[19,33-36] Modifications to the polymer composition conventionally avoid disrupting the π-conjugated backbone; most efforts aimed at improving solution processability and mechanical properties have instead focused on altering the composition and structure of the side chains or blending the π-conjugated polymers with other more flexible polymers.[1,2] However, studies of diblock and triblock copolymers composed of both semiconducting and electrically insulating species suggest that the purposeful disruption of the π-conjugated pathway with nonconjugated moieties can lead to polymer-based OSC that retain effective charge-carrier mobilities while being more flexible and solution processable.[37-42]

For instance, early efforts to design and characterize semiconducting diblock copolymers comprised of polyethylene and regioregular poly(3-hexylthiophene) (P3HT) led to materials with robust mechanical properties and reasonable charge carrier mobilities (on the order of 10^{-2} $cm^2V^{-1}s^{-1}$), even with high polyethylene loadings.[43,44] Similarly, recent polymer designs incorporate small nonconjugated alkyl segments (conjugation breaks) directly into the repeat unit of the otherwise π-conjugated polymer, which then demonstrate ready solution or melt processability and mechanical properties desirable for deformable, polymer-based OSC. Semiconducting polymer thin films composed of π-conjugated polymers with conjugation break spacers (CBS), sometimes blended with a small amount of fully π-conjugated polymer have also shown increased solubility, improved melt processability, charge-carrier mobilities on the order of 1 $cm^2V^{-1}s^{-1}$, and thermal healing of defects.[45-66] The inclusion of CBS units has also been shown to improve a wide range of mechanical properties without significantly compromising the optoelectronic characteristics, including increasing ductility and decreasing elastic modulus, increasing toughness and fracture strain, and reducing the glass transition temperature of the polymer OSC.[60-62,67,68]

In this work, we seek to clarify the effect of alkyl-based CBS segments on polymer structure, dynamics, and thermal properties in the solid state. We perform atomistic molecular dynamics (MD) simulations to examine a family of polymers based on diketopyrrolopyrrole-tetrathiophene (DPP-4T) previously synthesized by Mei et al.[47-54,60] While some atomistic and coarse-grained MD techniques have previously been used to study dynamics of conjugated polymer systems at various scales,[69-73] here we demonstrate atomistic MD simulations of polymer melts comprised of hundreds of polymer chains, with experimentally relevant individual chain molecular weights (>700,000 atoms per system), for dozens of nanoseconds. As shown in Figure 1, we consider DPP-

4T and ten variations here labeled DPP-CBS-*m*, where *m* represents the number of methylene units in the CBS segment. Using these eleven polymers, we examine the effect of *m* on: (i) vacuum-phase dynamics; (ii) chain structures, diffusivity, and glass transition of single-component polymer glasses and melts; and (iii) chain structures and diffusivity of fully conjugated DPP-4T polymers blended into DPP-CBS-*m*.

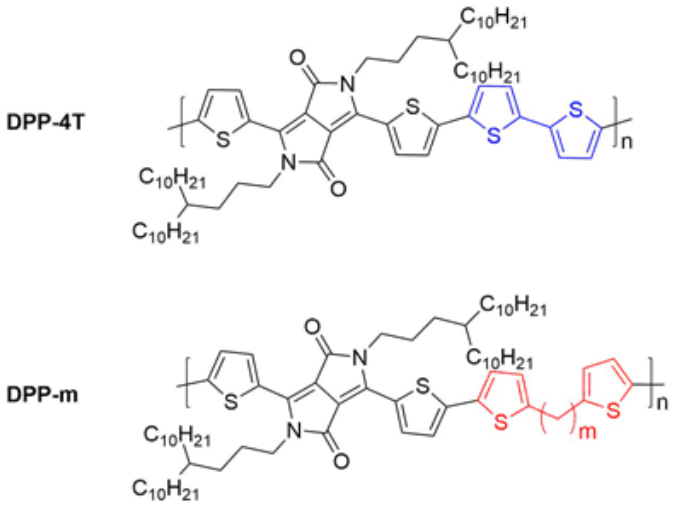

Figure 1. Chemical structures of DPP-4T and the DPP-CBS-*m* polymers examined in this study.

Computational Methods

Atomistic molecular dynamics (MD) simulations were performed with the GROMACS 2020 software suite.[74-82] Bond stretch and angle bend potential parameters were adapted from either the OPLS-AA parameter set[83,84] or adapted from the polythiophene parameterization of Huang et al.[85] Atomic charges and dihedral angle torsion potentials were parameterized via density functional theory (DFT) calculations. Parameter files containing the bonded interactions and molecular topology of single DPP-4T and DPP-CBS-*m* chains are available in the Supporting Information (SI), along with more details of the DPP dihedral angle parameterization.

DFT calculations were performed using the Gaussian 16 Rev. A.03 software suite.[86] DPP-4T and DPP-CBS-*m* trimers were optimized at the OT-ωB97X-D/6-31G(d) level of theory. Tuned ω values are available in Table S1 in the SI. Empirical gap tuning was performed for each trimer following the methodology of Sun et al.[87] Atomic charges were calculated at the same level of theory using the Charge Model 5 (CM5) framework.[88,89]

The DPP-4T chains each consisted of 20 monomers, while the DPP-CBS-*m* chains each consisted of 10 monomers. Details of these species, such as the molecular weights and radii of gyration in the extended conformations, are available in Table S2. A short-range cutoff of 1.4 nm was used for all MD simulations, with long-range interactions calculated via particle mesh Ewald summation. Hydrogen bonds were constrained via LINCS to their equilibrium values.

To examine the isolated-chain dynamics, an extended chain conformation was inserted at the center of an empty cubic simulation box with the side lengths equal to the end-to-end chain length plus 4 nm. Following an initial energy minimization, each system was allowed to evolve for 2 ns of NVT dynamics at 300 K. Energy minimization was performed using the conjugate-gradient method with a convergence threshold of 1000 kJ/mol/nm total force. MD were performed using a leapfrog integrator with time step 1 fs and a velocity-rescaling thermostat with coupling constant 0.1 ps.

To prepare each condensed-phase system, a chain was inserted at the center of an empty cubic simulation box with the side lengths equal to the end-to-end length of the fully extended chain conformation plus 10 nm. Next, a predetermined number of chains were inserted into the cell at random positions and orientations while ensuring no polymer overlap. The number of chains to be inserted was dependent on the molecular weight of the chains themselves. Multi-component

systems were prepared with a composition of 95% DPP-CBS-*m* and 5% DPP-4T by weight. In both single- and multi-component systems, all input structures of a given species were identical. The total molecular weight of the simulation cell was kept approximately constant, corresponding to 200 chains of molecular weight 22.7 kDa for single-component DPP-4T and a range of approximately 400–360 chains of molecular weights 11.5–12.8 kDa for single-component DPP-CBS-1 through DPP-CBS-10, respectively. Complete details of the single- and multi-component systems are given in Tables S3 and S4, but we note that the polymer chain masses are consistent with those synthesized in experiment.[49]

To prepare polymer glasses or melts with densities and structures representative of experiment, we adapted the procedure developed by Larsen et al.,[90] itself a refinement of similar techniques published earlier by Hofmann et al. and by Karayiannis et al.[91,92] After polymer chain insertion, the single- and multi-component glasses were taken through a 19-step process during which the system is repeatedly heated and cooled as the system is rapidly compressed to a maximum pressure of 50 kbar before returning to 1 bar. The process consists of a series of thermal cycles, each containing one low-temperature NPT compression step followed by two NVT steps at 1 bar, first at high temperature and then at low temperature. Specific details of each step are given in Table S5. This process of thermal and pressure shocks both mitigates the impact of initial conformational bias and provides thermal energy to escape kinetic traps which can otherwise prevent conformations from evolving over time. All steps used a leapfrog integrator with time step 2 fs and a velocity-rescaling thermostat with coupling constant 0.1 ps. NPT steps used a Berendsen barostat with isotropic pressure coupling and coupling constant 2.0 ps. After the 19-step procedure, each simulation box represents an amorphous condensed-phase system at 300 K and 1 bar with realistic density and polymer structures.

Next, each condensed-phase system was heated to 600 K over 2 ns, then held at 600 K and 1 bar for 8 ns for equilibration. Each of these steps was performed using a velocity-rescaling thermostat with coupling constant 0.1 ps and a Berendsen barostat with coupling constant 1 ps. After equilibration, the system was held at 600 K and 1 bar for 10 ns of production MD using a Nosé-Hoover thermostat with coupling constant 0.1 and a Parrinello-Rahman barostat with isotropic pressure coupling and coupling constant 1.0 ps. The system was then cooled to 300 K at a rate of 50 K/ns using the same Nosé-Hoover thermostat and Parrinello-Rahman barostat used for the previous step. Finally, the system was held at 300 K and 1 bar for 8 ns of equilibration using a velocity-rescaling thermostat and a Berendsen barostat, followed by 10 ns of production MD using a Nosé-Hoover thermostat and a Parrinello-Rahman barostat as before.

To estimate the glass transitions of the single-component systems, a snapshot of each system was taken following the 10 ns MD production at 600 K. This system was cooled to 50 K at a rate of 15 K/ns using a Nosé-Hoover thermostat and a Parrinello-Rahman barostat with the same properties as those discussed above. The system pressure was held at 1 bar throughout the cooling step. Due to the time required for this cooling procedure, this step was performed only on the single-component systems.

Results and Discussion

Isolated Chain Dynamics

We begin by analyzing of the structure and dynamics of isolated polymer chains in vacuum. Polymer chains in vacuum may be regarded as being surrounded by a very poor solvent; thus, we expect extended chains to collapse and self-solvate in order to maximize intra-molecular

interactions. Simulations of this process help to clarify the effects of the CBS segment length, *m*, on the chain dynamics. As a note on clarity, to distinguish the DPP-CBS-m species more easily from DPP-4T, we will refer to them in brief as CBS-*m*.

Figure 2 shows the radii of gyration (R_g) of the polymer chains in vacuum as a function of time, as well as a series of representative chain conformations. Each line represents the average of three independent vacuum simulations beginning from extended conformations. The CBS-*m* systems collapse more quickly than the DPP-4T system (as indicated by the slope of the steady-state collapse region of each line). Similarly, the chains with smaller *m* generally collapse more quickly than those with larger *m*. Close inspection of Figure 2 also suggests an alternation in the CBS-*m* collapse rates based on the parity of *m*. Both the CBS-2 and the CBS-3 systems begin from similar R_g, yet CBS-2 collapses more slowly than CBS-3. Likewise, CBS-4 and CBS-5 begin from similar R_g, but CBS-4 collapses far more slowly than CBS-5, as well as the even longer CBS-7 and CBS-9.

Notably, similar odd/even alternation of properties in OSC has previously been reported in literature. Mei and co-workers[49] observed that semicrystalline films made of DPP-CBS polymers with odd numbered CBS exhibit lower melting transitions, smaller π-π stacking distances, two-dimensional lamellar-like morphologies, and higher degrees of crystallinity. These variations were attributed to the odd/even alternation by differences in the packing of the aromatic blocks in the crystalline regions, resulting from the relative orientation of the blocks imposed by the CBS segment, as was also observed for dimers of conjugated moieties connected by an alkyl spacer.[93] However, this explanation does not apply to isolated polymer chains, which do not exhibit any crystalline aggregates. An alternative mechanism, which has been demonstrated for alkyl chains in solution, links the odd/effect to alkyl chain conformations and their population,[94,95] in alignment

with our observations that isolated odd and even CBS-m polymer chains have different sizes of the conformational space they can populate.

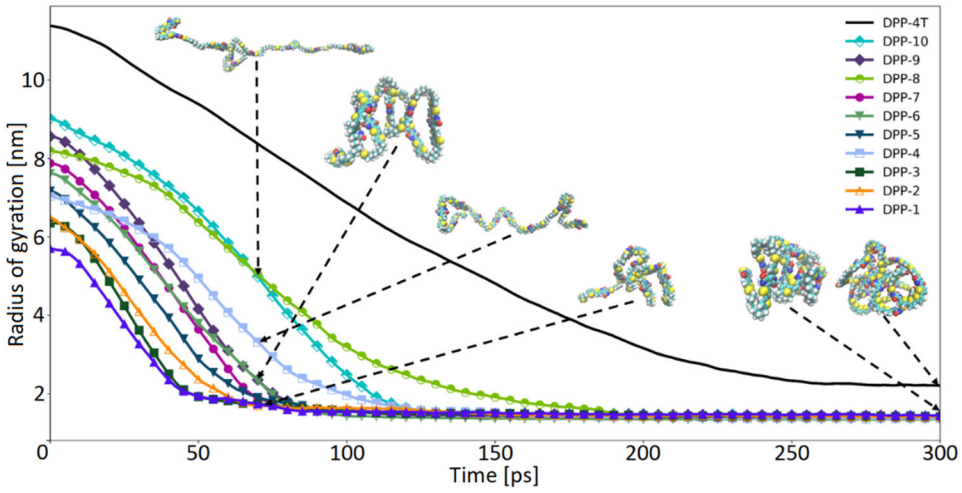

Figure 2. Radii of gyration during the first 300 ps of vacuum dynamics for the DPP-4T and DPP-CBS-*m* species.

To illustrate the effect of *m* more clearly on the chain collapse rates, we first determine the rate of chain collapse by extracting the slopes from least-squares linear regression models applied to the (approximately) steady-state regime. Because the initial R_g values of the CBS-*m* chains vary with *m*, we then normalize the collapse rates by the radii of gyration of the chains in the maximally extended state, R_g^*. The R_g^* values and images of these conformations are available in Table S2 and Figure S4, respectively. (The R_g^* values differ slightly from the radii of gyration at time $t = 0$ ps in Figure 2, as the lines in Figure 2 represent the three-simulation average with three slightly different extended conformations.)

The normalized average collapse rates are displayed in Figure 3 with errors corresponding to the three-simulation standard deviations. Linear fits applied separately to the odd and even CBS-*m* families reveal that a CBS-*m* chain with a given odd *m* generally collapses more quickly than the

"adjacent" chains with even (m – 1) or (m + 1). It is also evident that the collapse rate decreases with increasing m. This can be rationalized by recognizing that chains with larger m are more flexible, as experimentally confirmed by Galuska et al.,[68] and have a larger conformational space to explore.

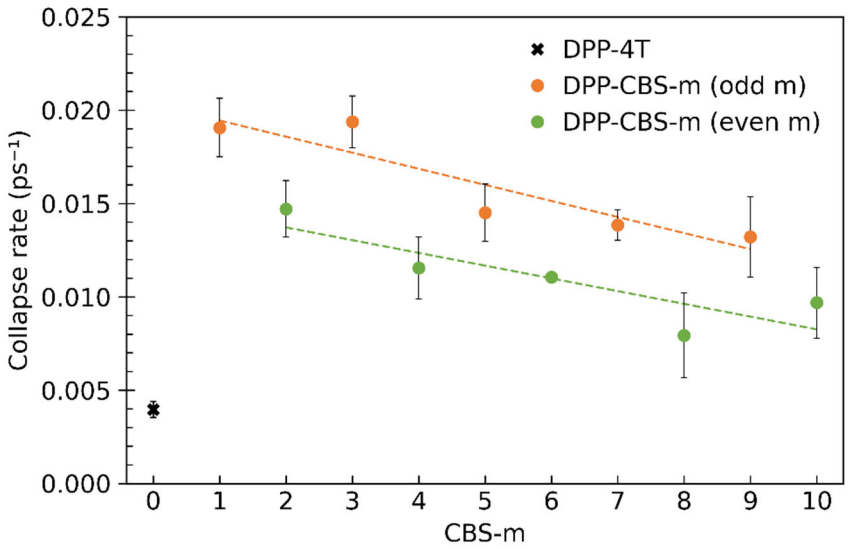

Figure 3. Normalized collapse rates of the DPP-4T and DPP-CBS-*m* species.

Single-Component Systems

With the insights gained from the isolated polymer chains in vacuum simulations, we now turn to single-component glass (SCG) and multi-component glass (MCG) systems. For convenience, we will use the nomenclature "SCG-*m*" to refer to the SCG system composed entirely of CBS-*m* (with $m = 0$ corresponding to the fully conjugated DPP-4T system). Likewise, the nomenclature "MCG-*m*" refers to the multi-component glass composed of 95% DPP-CBS-*m* and 5% DPP-4T. Additional discussion of this nomenclature is provided in the SI. The densities of these systems

decrease with m, as shown in Tables S3 and S4, from 1.075 g/cm^3 at 300 K for SCG-0 to 1.057 g/cm^3 for SCG-10. As is expected from the backbone chemistry, these densities fall between reported densities for π-conjugated polymers such as P3HT or PTB7 and those measured for amorphous polyethylene.[96,97]

To examine how the CBS segment length m affects the condensed-phase polymer chain structure and dynamics, we compute the average radius of gyration of each species. We focus on R_g values of the SCG systems calculated following production MD at device-relevant temperature of 300 K; the R_g values calculated from the production MD step at 600 K were higher than the corresponding values at 300 K by an average of approximately 3%. More compact chains in amorphous phases are associated with more flexible backbones, a potentially desirable scenario for intrinsically flexible and stretchable polymer materials. Figure 4a suggests that R_g increases with m for SCG-1 through SCG-10, with DPP-4T being larger due to the longer DPP-4T chains. As the CBS-m chains have different fully extended lengths (R_g^*), however, we normalize the computed R_g values by R_g^*. Figure 4b shows that the polymer chains in each system are more flexible (and thus collapse to a smaller fraction of their extended state) with increasing alkyl segment length, as intuition would suggest. The DPP-4T chains display surprising flexibility, although direct comparison with the CBS-m species is difficult as the DPP-4T chains were nearly twice as long as some of the CBS-m chains in the outstretched conformation. We also note that the normalized radii of gyration alternate depending on whether m is even or odd, similar to the collapse rates of the isolated chains in vacuum (see above).

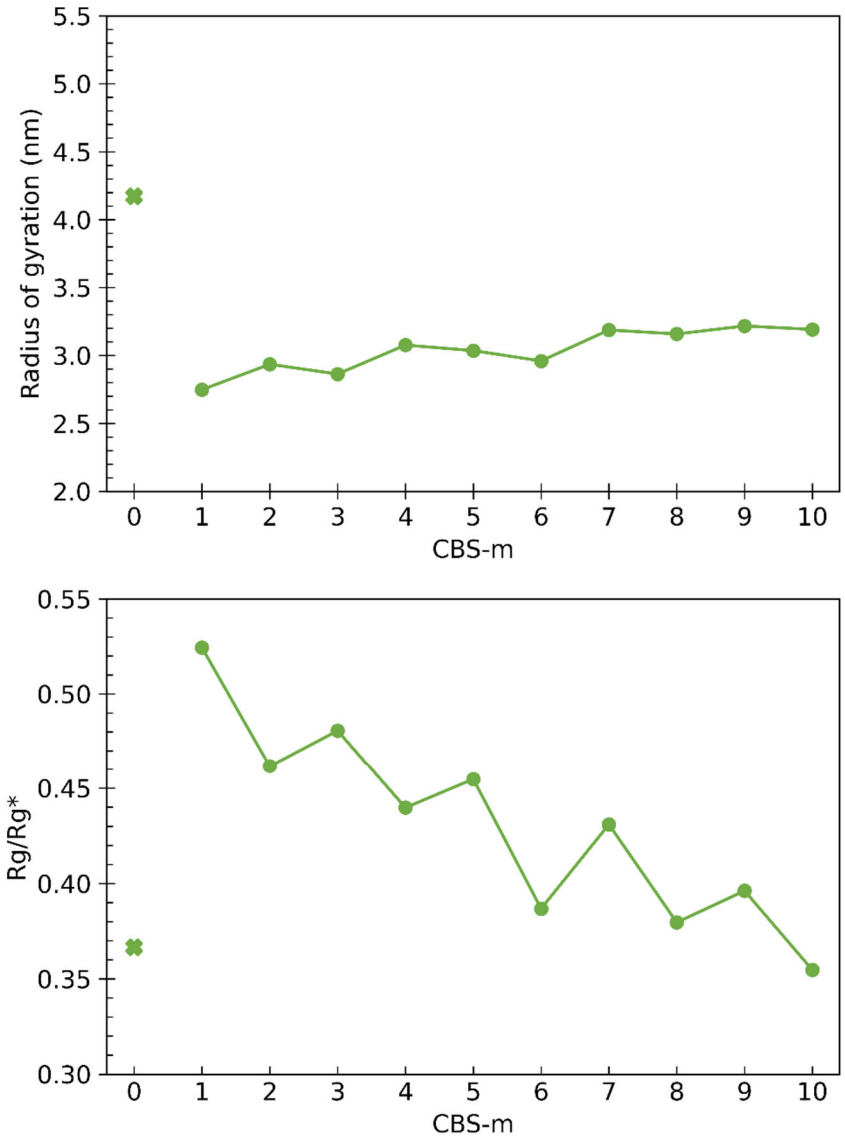

Figure 4. (Top) Radii of gyration (R_g) vs. number of methylene units (m) in π-conjugation break spacers (CBS) for the DPP-4T (marked with ×) and DPP-CBS-m single-component systems. (Bottom) Normalized radii of gyration (R_g/R_g^*) vs. m for the same species.

Mean squared displacement data for chains in the SCG systems during production MD were extracted to compare the self-diffusion coefficient of each species and study the impact of m on chain dynamics. MSD data were plotted as a function of time and a linear fit was applied to each system from t = 2 ns to 8 ns; the slopes of these models were used to determine the diffusivity.

Figure 5 shows the SCG diffusivities in the glass (300 K) and melt (600 K) states; exact values and a discussion of the error associated with these values are presented in Table S8. Average chain diffusivities are nearly two orders of magnitude higher in the melt, with chain diffusion significantly reduced in the glass. At 300 K, it is difficult to deconvolute the observed variability from thermal fluctuations and uncertainty in determining the diffusivity. At 600 K, however, diffusion proceeds much more rapidly, and the diffusivity increases with *m*; the stiffer and larger fully conjugated DPP-4T chains display a lower melt diffusivity than the CBS-*m* chains. (A more detailed plot showing only the diffusivities at 600 K of both the SCG and MCG systems is shown in Figure 8.)

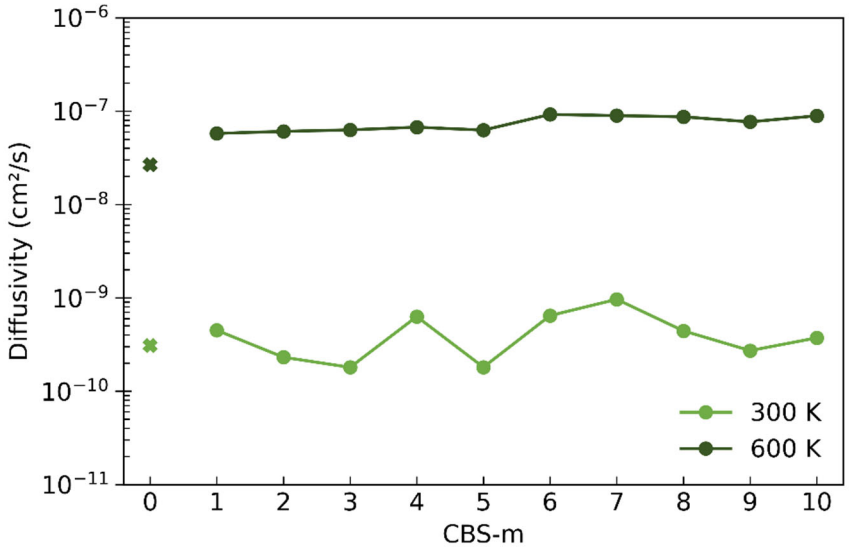

Figure 5. Diffusivity vs. number of methylene units (*m*) in π-conjugation break spacers (CBS) for the DPP-4T (marked with ×) and DPP-CBS-*m* single-component systems.

To probe the glass transition temperatures (T_g) of the SCG systems, the temperature and density of each system were measured throughout the cooling step from 600 K to 50 K. Linear fits were applied to the data to determine T_g as the temperature at which the thermal expansion coefficient

changes. An illustration of the method of determining T_g and a discussion of the related error are available in Figure S5. The cooling during this step was performed at a rate of 15 K/ns. The T_g values extracted from these simulations are shown in Figure 6, with exact T_g values and errors shown in Figure S5. The T_g data further illustrate the effect of m on the flexibility and on the thermomechanical properties of the SCG-m: The glass transitions are observed to shift toward lower temperatures as the length of the conjugation break increases (i.e., as the chain stiffness decreases), consistent with recent experiments.[68,98] We note that suppressed T_g with longer alkyl chains is also observed for chains appended to the periphery of polymer backbones, and is due to the internal plasticization of the backbone by these side chains.[99] Typically, two T_g are observed in π-conjugated polymers, with the side chain T_g being much lower than the backbone T_g. While the backbone T_g decreases with increasing alkyl chain length, the opposite is observed for the side chain T_g.[98] Such a scenario limits the control over the backbone T_g that can be achieved with side chain engineering alone. Moreover, the length of the side chains is limited by the need to avoid their crystallization. CBS provide an additional and more direct control over the backbone T_g. It is currently not clear, however, if the CBS segments will lead to a separate glass transition since they are directly part of the backbone.

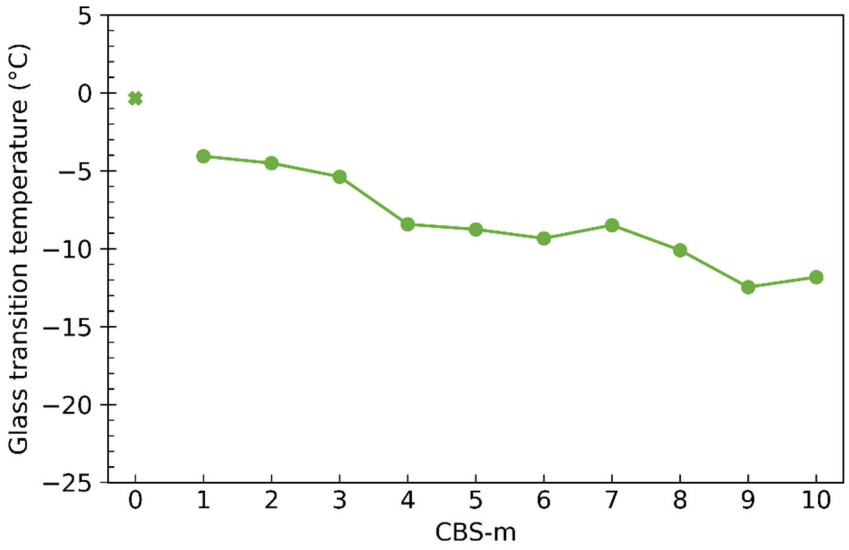

Figure 6. Glass transition temperature (T_g) vs. number of methylene units (m) in π-conjugation break spacers (CBS) for the DPP-4T (marked with ×) and DPP-CBS-*m* single-component systems.

The glass transition of DPP-4T has been found to occur near or slightly below room temperature,[100] with a T_g value of 6.8 °C measured through dynamic mechanical analysis.[101] In addition, differential scanning calorimetry and rheological experiments performed by Xie et al. on a wide range of conjugated polymers have revealed that T_g decreases with increasing side chain weight ratio, with different trends for thiophene-rich and phenyl-rich polymers.[98] Based on the study by Xie et al., a side chain weight ratio of approximately 58% is predicted to result in a T_g value near 0 °C.[98] Here, the fully π-conjugated, thiophene-rich DPP-4T polymer has a side-chain ratio of approximately 60% by mass and a T_g value of just under 0 °C, with T_g decreasing as the CBS length is increased (contributing to increasing aliphatic character), in excellent agreement with experimental T_g values.

Multi-Component Systems

Fully π-conjugated DPP-4T chains have been blended in small amounts with CBS-*m* chains for improved charge-carrier transport properties.[102] Here we analyze the structure and dynamics of DPP-4T chains in this blend environment, and how these might be affected by the CBS segment length of surrounding chains. Although DPP-4T comprises only 5% of each multi-component system by weight, including this relatively small amount of fully π-conjugated species has a noticeable impact on chain flexibility in the bulk phase. The normalized radii of gyration (R_g/R_g^*) of the MCG systems in Figure 7 demonstrate that the DPP-4T chains in each system behave more similarly to their CBS-*m* counterparts in the MCG systems than in the SCG systems. The non-normalized R_g values are shown in Figure S6. The large difference between CBS-1 and DPP-4T observed in the SCG is significantly reduced in the MCG. Indeed, the DPP-4T chains remain more extended and collapse less in each MCG than in the pure DPP-4T SCG. The CBS-*m* chains, meanwhile, are largely similar to their corresponding SCG; this is perhaps unsurprising, given many CBS-*m* chains still experience an environment similar to the pure SCG phase.

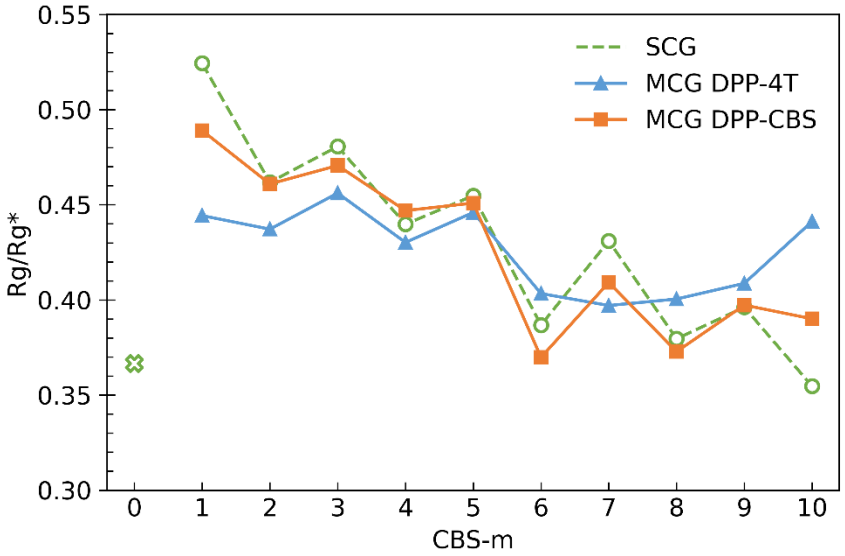

Figure 7. Normalized radii of gyration (R_g/R_g^*) vs. number of methylene units (*m*) in π-conjugation break spacers (CBS) for the multi-component systems. Single-component systems shown for reference (DPP-4T marked with ×).

The impact of the surrounding environment on the dynamics of the DPP-4T chains is illustrated further in Figure 8, which shows the diffusivities of the MCG at 600 K; the SCG are shown with dashed lines for reference. The diffusivities of the DPP-4T chains in the MCG are all elevated compared to those in the pure DPP-4T SCG. The CBS-*m* chain dynamics in the MCG are largely similar to those in the corresponding SCG, although chains with small *m* appear to be slightly more mobile in the MCG, with an overall upward trend in diffusivity as a function of *m*. Diffusion at 300 K is again highly reduced, with no prevailing trends in diffusivity as a function of *m*, as shown in Figure S7.

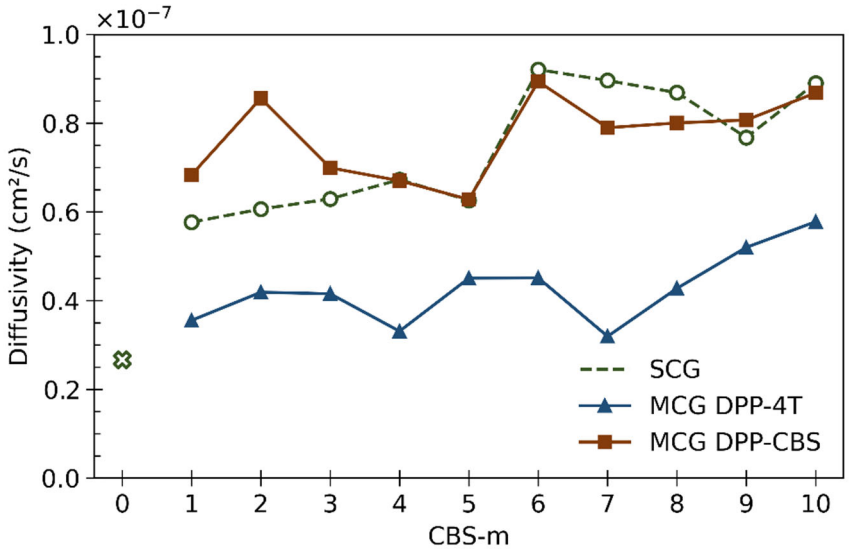

Figure 8. Diffusivity vs. number of methylene units (*m*) in π-conjugation break spacers (CBS) for the multi-component systems at elevated temperature (600 K). Single-component systems shown for reference (DPP-4T marked with ×).

As an alternative view of the data shown above, Figure 9 shows the diffusivity of the SCG and MCG plotted against R_g/R_g^*. The DPP-4T SCG is marked with a black cross; for the other species, the value of *m* is represented by the marker color, with saturation decreasing with increasing *m*. A plot of diffusivity against the unnormalized R_g values is shown in Figure S8. While the DPP-CBS-

m chains behave similarly in the SCG and MCG, the DPP-4T chains display considerably improved diffusion when blended with the DPP-CBS-*m* species.

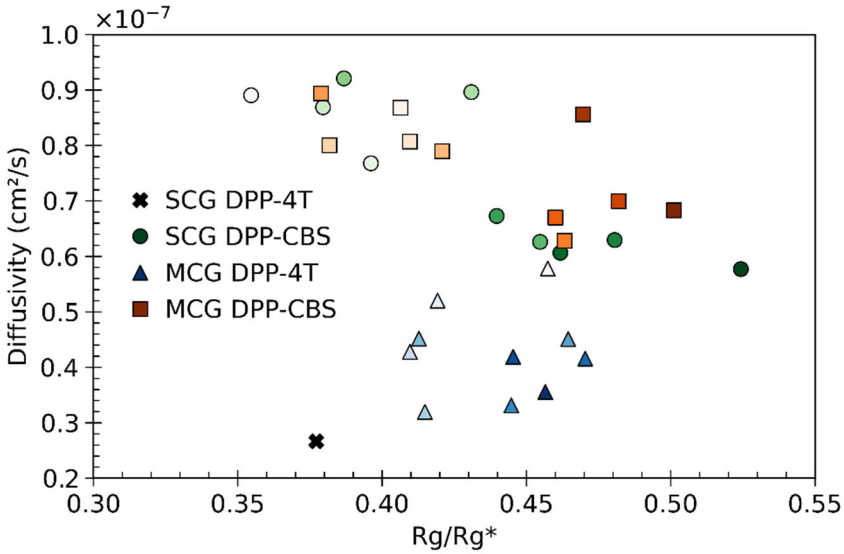

Figure 9. Diffusivity vs. normalized radius of gyration (R_g/R_g^*) for the single- and multi-component systems. The effect of chain environment on the mechanical properties of the chain is illustrated well by the difference between the single-component DPP-4T system (marked with ×) and the DPP-4T chains in the multi-component systems (marked with ▲).

Conclusion

MD simulations were used to analyze the effect of purposeful disruption of the π-conjugation pathway in the donor-acceptor semiconducting polymer DPP-4T. We examined the effect of introducing conjugation break spacers (CBS) between DPP-4T monomers on the polymer structure, dynamics, and thermal properties. Notably, our simulations of DPP-4T-based polymer glasses and melts make use of chain molecular weights relevant to and consistent with experiments.

We observe that incorporating CBS segments consisting of a linear series of *m* methylene units along the polymer backbone between π-conjugated monomers promotes flexibility, as intuition

suggests. In bulk simulations of polymer glasses and melts, DPP-CBS-*m* chains with larger *m* collapse to a smaller fraction of their extended length, with larger *m* also contributing to higher diffusivity and lower glass transition temperature. Moreover, when fully conjugated DPP-4T chains are blended in small proportion with DPP-CBS-*m* chains, we observe improved flexibility and elevated diffusion of the relatively stiff DPP-4T chains, with negligible impact on the DPP-CBS-*m* chains.

Our large-scale MD simulations provide a method to connect the atomistic-scale monomer chemistry of polymer chains with experimentally relevant molecular weights to some of the thermomechanical properties of the bulk-phase material. Models that connect charge-carrier transport to these large-scale atomistic simulations are the subject of ongoing work, while future efforts will expand the studied thermomechanical properties of this protocol to include stress–strain relationships. Nonetheless, the effects of breaking the backbone π-conjugation pathway on bulk-phase material characteristics suggest an avenue for developing polymer-based semiconductors with both desirable semiconductor characteristics and enhanced processability and deformability.

Supporting Information

Supporting Information is available from the Wiley Online Library.

Acknowledgements

We thank Dr. Jianguo Mei for fruitful discussions as this project progressed. This work was supported in part by the Office of Naval Research (Award Nos. N00014-16-1-2985 and N00014-18-1-2448) and the National Science Foundation under Cooperative Agreement No. 1849213. Supercomputing resources were provided by the Department of Defense (DoD) through the DoD High Performance Computing Modernization Program (HPCMP; Project No. ONRDC40433481) and by the University of Kentucky Information Technology Department and Center for Computational Sciences (CCS).

Notes

Connor Callaway and Joel Bombile contributed equally to the project and manuscript.

The authors declare no competing financial interest.

Received: ((will be filled in by the editorial staff))
Revised: ((will be filled in by the editorial staff))
Published online: ((will be filled in by the editorial staff))

References

1. M. U. Ocheje, B. P. Charron, A. Nyayachavadi, S. Rondeau-Gagné. *Flexible and Printed Electronics* **2017**, *2*, 043002.

2. S. E. Root, S. Savagatrup, A. D. Printz, D. Rodriquez, D. J. Lipomi. *Chemical Reviews* **2017**, *117*, 6467-6499.

3. B. Kang, F. Ge, L. Qiu, K. Cho. *Advanced Electronic Materials* **2017**, *3*, 1600240.

4. H. Tran, V. R. Feig, K. Liu, Y. Zheng, Z. Bao. *Macromolecules* **2019**, *52*, 3965-3974.

5. B. Wang, A. Facchetti. *Advanced Materials* **2019**, *31*, 1901408.

6. A. Facchetti. *Chemistry of Materials* **2011**, *23*, 733-758.

7. R. S. Kularatne, H. D. Magurudeniya, P. Sista, M. C. Biewer, M. C. Stefan. *Journal of Polymer Science Part A: Polymer Chemistry* **2013**, *51*, 743-768.

8. I. Osaka. *Polymer Journal* **2015**, *47*, 18-25.

9. T. M. Swager. *Macromolecules* **2017**, *50*, 4867-4886.

10. B. Zheng, L. Huo, Y. Li. *NPG Asia Materials* **2020**, *12*, 3.

11. J. Mei, Z. Bao. *Chemistry of Materials* **2014**, *26*, 604-615.

12. Z.-G. Zhang, Y. Li. *Science China Chemistry* **2015**, *58*, 192-209.

13. Y. Qiao, X. Yin, C. Tang. *Science China Chemistry* **2015**, *58*, 1641-1650.

14. K. Kremer, G. S. Grest. *The Journal of Chemical Physics* **1990**, *92*, 5057-5086.

15. D. Beljonne, G. Pourtois, C. Silva, E. Hennebicq, L. M. Herz, R. H. Friend, G. D. Scholes, S. Setayesh, K. Müllen, J. L. Brédas. *Proceedings of the National Academy of Sciences* **2002**, *99*, 10982.

16. Y.-s. Huang, S. Westenhoff, I. Avilov, P. Sreearunothai, J. M. Hodgkiss, C. Deleener, R. H. Friend, D. Beljonne. *Nature Materials* **2008**, *7*, 483-489.

17. K. Do, D. M. Huang, R. Faller, A. J. Moulé. *Physical Chemistry Chemical Physics* **2010**, *12*, 14735-14739.

18. Y. Olivier, D. Niedzialek, V. Lemaur, W. Pisula, K. Müllen, U. Koldemir, J. R. Reynolds, R. Lazzaroni, J. Cornil, D. Beljonne. *Advanced Materials* **2014**, *26*, 2119-2136.

19. N. E. Jackson, K. L. Kohlstedt, B. M. Savoie, M. Olvera de la Cruz, G. C. Schatz, L. X. Chen, M. A. Ratner. *Journal of the American Chemical Society* **2015**, *137*, 6254-6262.

20. N. R. Tummala, C. Bruner, C. Risko, J.-L. Brédas, R. H. Dauskardt. *ACS Appl. Mater. Interfaces* **2015**, *7*, 9957-9964.

21. T. J. Fauvell, T. Zheng, N. E. Jackson, M. A. Ratner, L. Yu, L. X. Chen. *Chemistry of Materials* **2016**, *28*, 2814-2822.

22. M. L. Jones, D. M. Huang, B. Chakrabarti, C. Groves. *The Journal of Physical Chemistry C* **2016**, *120*, 4240-4250.

23. S. Saiev, L. Bonnaud, P. Dubois, D. Beljonne, R. Lazzaroni. *Polymer Chemistry* **2017**, *8*, 5988-5999.

24. C. Luo, M. Kröger, J.-U. Sommer. *Polymer* **2017**, *109*, 71-84.

25. E. Mahmoudinezhad, A. Marquardt, G. Eggeler, F. Varnik. *Procedia Computer Science* **2017**, *108*, 265-271.

26. S. E. Root, N. E. Jackson, S. Savagatrup, G. Arya, D. J. Lipomi. *Energy & Environmental Science* **2017**, *10*, 558-569.

27. S. R. Chaudhari, J. M. Griffin, K. Broch, A. Lesage, V. Lemaur, D. Dudenko, Y. Olivier, H. Sirringhaus, L. Emsley, C. P. Grey. *Chemical Science* **2017**, *8*, 3126-3136.

28. K. Do, M. K. Ravva, T. Wang, J.-L. Brédas. *Chemistry of Materials* **2017**, *29*, 346-354.

29. L. Ye, H. Hu, M. Ghasemi, T. Wang, B. A. Collins, J.-H. Kim, K. Jiang, J. H. Carpenter, H. Li, Z. Li, T. McAfee, J. Zhao, X. Chen, J. L. Y. Lai, T. Ma, J.-L. Bredas, H. Yan, H. Ade. *Nature Materials* **2018**, *17*, 253-260.

30. D. R. Reid, N. E. Jackson, A. J. Bourque, C. R. Snyder, R. L. Jones, J. J. de Pablo. *The Journal of Physical Chemistry Letters* **2018**, *9*, 4802-4807.

31. S. M. Ryno, C. Risko. *Physical Chemistry Chemical Physics* **2019**, *21*, 7802-7813.

32. G. Han, X. Shen, R. Duan, H. Geng, Y. Yi. *Journal of Materials Chemistry C* **2016**, *4*, 4654-4661.

33. D. Hertel, U. Scherf, H. Bässler. *Advanced Materials* **1998**, *10*, 1119-1122.

34. X. Zhang, H. Bronstein, A. J. Kronemeijer, J. Smith, Y. Kim, R. J. Kline, L. J. Richter, T. D. Anthopoulos, H. Sirringhaus, K. Song, M. Heeney, W. Zhang, I. McCulloch, D. M. DeLongchamp. *Nature Communications* **2013**, *4*, 2238.

35. J. Lee, A. J. Kalin, T. Yuan, M. Al-Hashimi, L. Fang. *Chemical Science* **2017**, *8*, 2503-2521.

36. V. Lemaur, J. Cornil, R. Lazzaroni, H. Sirringhaus, D. Beljonne, Y. Olivier. *Chemistry of Materials* **2019**, *31*, 6889-6899.

37. G. Widawski, M. Rawiso, B. François. *Nature* **1994**, *369*, 387-389.

38. B. Karakaya, W. Claussen, K. Gessler, W. Saenger, A. D. Schlüter. *Journal of the American Chemical Society* **1997**, *119*, 3296-3301.

39. M. A. Hempenius, B. M. W. Langeveld-Voss, J. A. E. H. v. Haare, R. A. J. Janssen, S. S. Sheiko, J. P. Spatz, M. Möller, E. W. Meijer. *Journal of the American Chemical Society* **1998**, *120*, 2798-2804.

40. U. Stalmach, B. de Boer, C. Videlot, P. F. van Hutten, G. Hadziioannou. *Journal of the American Chemical Society* **2000**, *122*, 5464-5472.

41. J. Liu, E. Sheina, T. Kowalewski, R. D. McCullough. *Angewandte Chemie International Edition* **2002**, *41*, 329-332.

42. F. J. M. Hoeben, P. Jonkheijm, E. W. Meijer, A. P. H. J. Schenning. *Chemical Reviews* **2005**, *105*, 1491-1546.

43. C. P. Radano, O. A. Scherman, N. Stingelin-Stutzmann, C. Müller, D. W. Breiby, P. Smith, R. A. J. Janssen, E. W. Meijer. *Journal of the American Chemical Society* **2005**, *127*, 12502-12503.

44. C. Müller, S. Goffri, D. W. Breiby, J. W. Andreasen, H. D. Chanzy, R. A. J. Janssen, M. M. Nielsen, C. P. Radano, H. Sirringhaus, P. Smith, N. Stingelin-Stutzmann. *Advanced Functional Materials* **2007**, *17*, 2674-2679.

45. K. Van den Bergh, P. Willot, D. Cornelis, T. Verbiest, G. Koeckelberghs. *Macromolecules* **2011**, *44*, 728-735.

46. T. Erdmann, S. Fabiano, B. Milián-Medina, D. Hanifi, Z. Chen, M. Berggren, J. Gierschner, A. Salleo, A. Kiriy, B. Voit, A. Facchetti. *Advanced Materials* **2016**, *28*, 9169-9174.

47. Y. Zhao, X. Zhao, M. Roders, G. Qu, Y. Diao, A. L. Ayzner, J. Mei. *Chemistry of Materials* **2015**, *27*, 7164-7170.

48. Y. Zhao, X. Zhao, Y. Zang, C.-a. Di, Y. Diao, J. Mei. *Macromolecules* **2015**, *48*, 2048-2053.

49. X. Zhao, Y. Zhao, Q. Ge, K. Butrouna, Y. Diao, K. R. Graham, J. Mei. *Macromolecules* **2016**, *49*, 2601-2608.

50. Y. Zhao, X. Zhao, M. Roders, A. Gumyusenge, A. L. Ayzner, J. Mei. *Advanced Materials* **2016**, *29*, 1605056.

51. X. Zhao, G. Xue, G. Qu, V. Singhania, Y. Zhao, K. Butrouna, A. Gumyusenge, Y. Diao, K. R. Graham, H. Li, J. Mei. *Macromolecules* **2017**, *50*, 6202-6209.

52. Y. Zhao, A. Gumyusenge, J. He, G. Qu, W. W. McNutt, Y. Long, H. Zhang, L. Huang, Y. Diao, J. Mei. *Advanced Functional Materials* **2018**, *28*, 1705584.

53. A. Gumyusenge, X. Zhao, Y. Zhao, J. Mei. *ACS Appl. Mater. Interfaces* **2018**, *10*, 4904-4909.

54. A. Gumyusenge, X. Luo, H. Zhang, G. M. Pitch, A. L. Ayzner, J. Mei. *ACS Appl. Polym. Mater.* **2019**, *1*, 1778-1786.

55. B. C. Schroeder, Y.-C. Chiu, X. Gu, Y. Zhou, J. Xu, J. Lopez, C. Lu, M. F. Toney, Z. Bao. *Advanced Electronic Materials* **2016**, *2*, 1600104.

56. D. Fong, A. Adronov. *Macromolecules* **2017**, *50*, 8002-8009.

57. J. Mun, G.-J. N. Wang, J. Y. Oh, T. Katsumata, F. L. Lee, J. Kang, H.-C. Wu, F. Lissel, S. Rondeau-Gagné, J. B. H. Tok, Z. Bao. *Advanced Functional Materials* **2018**, *28*, 1804222.

58. A. Rahmanudin, L. Yao, K. Sivula. *Polymer Journal* **2018**, *50*, 725-736.

59. W.-J. Xiao, J. Wang, H.-J. Li, L. Liang, X. Xiang, X.-Q. Chen, J. Li, Z. Lu, W.-S. Li. *RSC Advances* **2018**, *8*, 23546-23554.

60. S. Savagatrup, X. Zhao, E. Chan, J. Mei, D. J. Lipomi. *Macromolecular Rapid Communications* **2016**, *37*, 1623-1628.

61. E. L. Melenbrink, K. M. Hilby, M. A. Alkhadra, S. Samal, D. J. Lipomi, B. C. Thompson. *ACS Appl. Mater. Interfaces* **2018**, *10*, 32426-32434.

62. E. L. Melenbrink, K. M. Hilby, K. Choudhary, S. Samal, N. Kazerouni, J. L. McConn, D. J. Lipomi, B. C. Thompson. *ACS Appl. Polym. Mater.* **2019**, *1*, 1107-1117.

63. G.-J. N. Wang, F. Molina-Lopez, H. Zhang, J. Xu, H.-C. Wu, J. Lopez, L. Shaw, J. Mun, Q. Zhang, S. Wang, A. Ehrlich, Z. Bao. *Macromolecules* **2018**, *51*, 4976-4985.

64. H.-J. Li, J.-T. Wang, C.-Y. Mei, W.-S. Li. *Chem. Commun.* **2014**, *50*, 7720-7722.

65. W. Shao, L. Liang, X. Xiang, H.-j. Li, F.-g. Zhao, W.-s. Li. *Chin. J. Chem* . **2015**, *33*, 847-851.

66. X. Xiang, W. Shao, L. Liang, X.-Q. Chen, F.-G. Zhao, Z. Lu, W. Wang, J. Li, W.-S. Li. *RSC Advances* **2016**, *6*, 23300-23309.

67. J. Y. Oh, S. Rondeau-Gagné, Y.-C. Chiu, A. Chortos, F. Lissel, G.-J. N. Wang, B. C. Schroeder, T. Kurosawa, J. Lopez, T. Katsumata, J. Xu, C. Zhu, X. Gu, W.-G. Bae, Y. Kim, L. Jin, J. W. Chung, J. B. H. Tok, Z. Bao. *Nature* **2016**, *539*, 411-415.

68. L. A. Galuska, W. W. McNutt, Z. Qian, S. Zhang, D. W. Weller, S. Dhakal, E. R. King, S. E. Morgan, J. D. Azoulay, J. Mei, X. Gu. *Macromolecules* **2020**, *53*, 6032-6042.

69. F. L. Lee, A. Barati Farimani, K. L. Gu, H. Yan, M. F. Toney, Z. Bao, V. S. Pande. *The Journal of Physical Chemistry Letters* **2017**, *8*, 5479-5486.

70. A. Melnyk, M. J. N. Junk, M. D. McGehee, B. F. Chmelka, M. R. Hansen, D. Andrienko. *The Journal of Physical Chemistry Letters* **2017**, *8*, 4155-4160.

71. C. M. Wolf, K. H. Kanekal, Y. Y. Yimer, M. Tyagi, S. Omar-Diallo, V. Pakhnyuk, C. K. Luscombe, J. Pfaendtner, L. D. Pozzo. *Soft Matter* **2019**, *15*, 5067-5083.

72. S. Zhang, A. Alesadi, M. Selivanova, Z. Cao, Z. Qian, S. Luo, L. Galuska, C. Teh, M. U. Ocheje, G. T. Mason, P. B. J. St. Onge, D. Zhou, S. Rondeau-Gagné, W. Xia, X. Gu. *Advanced Functional Materials* **2020**, *30*, 2002221.

73. S. Zhang, A. Alesadi, G. T. Mason, K.-L. Chen, G. Freychet, L. Galuska, Y.-H. Cheng, P. B. J. St. Onge, M. U. Ocheje, G. Ma, Z. Qian, S. Dhakal, Z. Ahmad, C. Wang, Y.-C. Chiu, S. Rondeau-Gagné, W. Xia, X. Gu. *Advanced Functional Materials* **2021**, *31*, 2100161.

74. H. Bekker, H. Berendsen, E. Dijkstra, S. Achterop, R. Vondrumen, D. Vanderspoel, A. Sijbers, H. Keegstra, M. Renardus, In PHYSICS COMPUTING '92; World Scientific Publishing: London, England, UK, **1993**, pp 252-256.

75. H. J. C. Berendsen, D. van der Spoel, R. van Drunen. *Computer Physics Communications* **1995**, *91*, 43-56.

76. E. Lindahl, B. Hess, D. van der Spoel. *Molecular modeling annual* **2001**, *7*, 306-317.

77. D. Van Der Spoel, E. Lindahl, B. Hess, G. Groenhof, A. E. Mark, H. J. C. Berendsen. *Journal of Computational Chemistry* **2005**, *26*, 1701-1718.

78. B. Hess, C. Kutzner, D. van der Spoel, E. Lindahl. *Journal of Chemical Theory and Computation* **2008**, *4*, 435-447.

79. S. Pronk, S. Páll, R. Schulz, P. Larsson, P. Bjelkmar, R. Apostolov, M. R. Shirts, J. C. Smith, P. M. Kasson, D. van der Spoel, B. Hess, E. Lindahl. *Bioinformatics (Oxford, England)* **2013**, *29*, 845-854.

80. S. Páll, M. J. Abraham, C. Kutzner, B. Hess, E. Lindahl. Solving Software Challenges for Exascale, Cham, 2015// 2015, pp 3-27.

81. M. J. Abraham, T. Murtola, R. Schulz, S. Páll, J. C. Smith, B. Hess, E. Lindahl. *SoftwareX* **2015**, *1-2*, 19-25.

82. Lindahl, Abraham, Hess, V. d. Spoel. *Zenodo* **2020**.

83. W. L. Jorgensen, J. Tirado-Rives. *Journal of the American Chemical Society* **1988**, *110*, 1657-1666.

84. W. L. Jorgensen, D. S. Maxwell, J. Tirado-Rives. *Journal of the American Chemical Society* **1996**, *118*, 11225-11236.

85. D. M. Huang, R. Faller, K. Do, A. J. Moulé. *Journal of Chemical Theory and Computation* **2010**, *6*, 526-537.

86. M. J. Frisch, G. W. Trucks, H. B. Schlegel, G. E. Scuseria, M. A. Robb, J. R. Cheeseman, G. Scalmani, V. Barone, G. A. Petersson, H. Nakatsuji, X. Li, M. Caricato, A. V. Marenich, J. Bloino, B. G. Janesko, R. Gomperts, B. Mennucci, H. P. Hratchian, J. V. Ortiz, A. F. Izmaylov, J. L. Sonnenberg, Williams, F. Ding, F. Lipparini, F. Egidi, J. Goings, B. Peng, A. Petrone, T. Henderson, D. Ranasinghe, V. G. Zakrzewski, J. Gao, N. Rega, G. Zheng, W. Liang, M. Hada, M. Ehara, K. Toyota, R. Fukuda, J. Hasegawa, M. Ishida, T. Nakajima, Y. Honda, O. Kitao, H. Nakai, T. Vreven, K. Throssell, J. A. Montgomery Jr., J. E. Peralta, F. Ogliaro, M. J. Bearpark, J. J. Heyd, E. N. Brothers, K. N. Kudin, V. N. Staroverov, T. A. Keith, R. Kobayashi, J. Normand, K. Raghavachari, A. P. Rendell, J. C. Burant, S. S. Iyengar, J. Tomasi, M. Cossi, J. M. Millam, M. Klene, C. Adamo, R. Cammi, J. W. Ochterski, R. L. Martin, K. Morokuma, O. Farkas, J. B. Foresman, D. J. Fox. Gaussian, Inc.: Wallingford, CT, **2016**.

87. H. Sun, S. Ryno, C. Zhong, M. K. Ravva, Z. Sun, T. Körzdörfer, J.-L. Brédas. *Journal of Chemical Theory and Computation* **2016**, *12*, 2906-2916.

88. A. V. Marenich, S. V. Jerome, C. J. Cramer, D. G. Truhlar. *Journal of Chemical Theory and Computation* **2012**, *8*, 527-541.

89. J.-D. Chai, M. Head-Gordon. *Physical Chemistry Chemical Physics* **2008**, *10*, 6615-6620.

90. G. S. Larsen, P. Lin, K. E. Hart, C. M. Colina. *Macromolecules* **2011**, *44*, 6944-6951.

91. D. Hofmann, L. Fritz, J. Ulbrich, C. Schepers, M. Böhning. *Macromolecular Theory and Simulations* **2000**, *9*, 293-327.

92. N. C. Karayiannis, V. G. Mavrantzas, D. N. Theodorou. *Macromolecules* **2004**, *37*, 2978-2995.

93. L. Ding, H.-B. Li, T. Lei, H.-Z. Ying, R.-B. Wang, Y. Zhou, Z.-M. Su, J. Pei. *Chemistry of Materials* **2012**, *24*, 1944-1949.

94. H. Izumi, S. Yamagami, S. Futamura, L. A. Nafie, R. K. Dukor. *Journal of the American Chemical Society* **2004**, *126*, 194-198.

95. J. A. Pradeilles, S. Zhong, M. Baglyas, G. Tarczay, C. P. Butts, E. L. Myers, V. K. Aggarwal. *Nature Chemistry* **2020**, *12*, 475-480.

96. G. M. Newbloom, K. M. Weigandt, D. C. Pozzo. *Soft Matter* **2012**, *8*, 8854-8864.

97. O. Dyck, S. Hu, S. Das, J. Keum, K. Xiao, B. Khomami, G. Duscher. *Polymers* **2015**, *7*.

98. R. Xie, A. R. Weisen, Y. Lee, M. A. Aplan, A. M. Fenton, A. E. Masucci, F. Kempe, M. Sommer, C. W. Pester, R. H. Colby, E. D. Gomez. *Nature Communications* **2020**, *11*, 893.

99. F. Sugiyama, A. T. Kleinschmidt, L. V. Kayser, D. Rodriquez, M. Finn, M. A. Alkhadra, J. M. H. Wan, J. Ramírez, A. S. C. Chiang, S. E. Root, S. Savagatrup, D. J. Lipomi. *Polymer Chemistry* **2018**, *9*, 4354-4363.

100. Z. Qian, Z. Cao, L. Galuska, S. Zhang, J. Xu, X. Gu. *Macromol. Chem. Phys.* **2019**, *220*, 1900062.

101. T. Sun, R. Song, N. Balar, P. Sen, R. J. Kline, B. T. O'Connor. *ACS Appl. Mater. Interfaces* **2019**, *11*, 3280-3289.

102. R. Noriega, J. Rivnay, K. Vandewal, F. P. V. Koch, N. Stingelin, P. Smith, M. F. Toney, A. Salleo. *Nature Materials* **2013**, *12*, 1038-1044.

TOC

The table of contents entry should be ~75 words long and should be written in the present tense. The text should be different from the abstract text.

Connor Callaway, Joel H. Bombile, Walker Mask, Sean M. Ryno, Chad Risko*

Thermomechanical Enhancement of DPP-4T through Purposeful π-Conjugation Disruption